Available online at www.sciencedirect.com

ScienceDirect

Solar Energy 122 (2015) 97–103

SOLAR ENERGY

www.elsevier.com/locate/solener

# High reproducibility of perovskite solar cells via a complete spin-coating sequential solution deposition process

Zhirong Zhang [a,b], Dong Wei [a], Bixia Xie [a], Xiaopeng Yue [a,c], Meicheng Li [a,*], Dandan Song [a], Yingfeng Li [a]

[a] State Key Laboratory of Alternate Electrical Power System with Renewable Energy Sources, North China Electric Power University, Beijing 102206, China

[b] School of Physics and Electromechanical Engineering, HeXi University, Zhangye, Gansu 734000, China

[c] Key Laboratory of Resource Exploration Research of Hebei Province, Hebei University of Engineering, Handan, Hebei 056038, China

Received 18 June 2015; received in revised form 29 July 2015; accepted 18 August 2015

Communicated by: Associate Editor Gion Calzaferri

**Abstract**

The controllability of conditions and parameters, in a certain procedure that adopted to prepare perovskite absorption layer, play a crucial role in morphology and crystallization of the resulting films, which is of great impact on the reproducibility of solar cells. Here we propose a complete spin-coating sequential solution deposition (spinning-SSD) process, in which a high concentration $CH_3NH_3I$ precursor was spin-coated on $PbI_2$-coated substrate insteading of immersing procedure; the pristine isopropanol was spin-coated to ameliorate the surface morphology and improve the quality of the resulting $CH_3NH_3PbI_3$ films both before and after the spin-coating of $CH_3NH_3I$ solution. Utilizing this spinning-SSD process, we fabricated meso-structured perovskite solar cells, and these devices exhibited decent performance and high reproducibility, achieving an average power conversion efficiency of 11.3% with the standard deviation as low as ±0.52. This optimized approach is expected to be used for fabricating high-performance perovskites solar cells with a full printable process.



*Keywords:* Perovskite; Solar cells; Reproducibility; Sequential solution deposition process

## 1. Introduction

Since the year of 2009, hybrid organic–inorganic perovskites were first introduced to the photovoltaic community (Kojima et al., 2009), perovskites solar cells (PSCs) based on such materials have garnered considerable attention due to their low cost and decent power conversion efficiency (PCE) (Burschka et al., 2013; Jeon et al., 2015; Kim et al., 2012; Lee et al., 2012; Liu et al., 2013; Tathavadekar et al., 2015; Yang et al., 2015). In general, a typical PSCs consists of three effective layers, including two contact layers that transport electrons and holes, respectively, a methylamine lead halide perovskite absorption layer sandwiched between of them (either with or without mesoporous metal oxide scaffold). Correspondingly, the performance of PSCs greatly depends on the properties and the qualities of these films. Up to now, great progress has been made on each isolated layer, with major emphasis on its processing and relevant material design. As far as the fabrication of perovskite films is concerned, several deposition methods have been reported, such as one-step solution deposition (Lee et al., 2012), sequential solution deposition

* Corresponding author.

http://dx.doi.org/10.1016/j.solener.2015.08.028
0038-092X/

(SSD) (Burschka et al., 2013), vacuum vapor deposition (Liu et al., 2013). By comparison, SSD process was found to exhibit better photovoltaic performance due to better morphology and interfaces, so it was paid more attention and used most widely. In a typical SSD method (call it as dipping-SSD later in this article), $PbI_2$ solution (e.g., dissolved in N,N-dimethylformamide (DMF)) was first spin-coated on the mesoporous or planar substrate, followed by dipping into $CH_3NH_3I$ (MAI) dissolved in isopropanol (IPA) solution (MAI/IPAs) to enable the reaction of $PbI_2$ and MAI to form the $CH_3NH_3PbI_3$ ($MAPbI_3$) perovskite. Such a process would consume a lot of materials, even worse, it led to the uncontrollability of process parameters in whole procedure, resulting in a large standard deviation ($\sim\pm2.0$) of reproducibility of PSCs fabrication (Burschka et al., 2013). In addition, MAI/IPAs must be refreshed hourly even after the immersion of only one substrates to ensure the same concentration of precursor solution, which caused more waste and trivia. Fortunately, when $PbI_2$-coated substrates were spin-coated with MAI/IPAs, not only the above-mentioned trivial/waste was avoided, but also the size controllability of the $MAPbI_3$ cuboids was obtained (Im et al., 2014; Xiao et al., 2014). While, we found that it made $MAPbI_3$ films tend to be nonuniform and the irregular pattern can be observed clearly. What's more, the existence of $PbI_2$ was detected by the X-ray diffraction (XRD) pattern analysis, which led to deteriorated devices due to its poor optical absorption properties as well as recombination of free charges generated in the perovskite phase (Zhao et al., 2014).

In this article, we propose more optimization measures to solve above-mentioned problems, including employing high concentration MAI/IPAs, spin-coating the pristine IPA both before and after coating of MAI/IPAs. By these ways, the resulting PSCs (adopted the structure of FTO glass/compact $TiO_2$/mesoporous $TiO_2$/$MAPbI_3$/Spiro-MeOTAD/Au) achieved an average efficiency of 11.3% with a small standard deviation ($\sim\pm0.52$). Furthermore, this spinning-SSD process is expected to use to fabricate high performance perovskites solar cells with a full printable procedure.

## 2. Experimental methods

### 2.1. Materials preparation

Unless stated otherwise, all reagents were purchased from Sigma Aldrich were used as received. Spiro-MeOTAD were purchased from Merk and used as received. MAI was synthesized according to a previous report (Lee et al., 2012). Methylamine ($CH_3NH_2$) solution 33 wt% in absolute ethanol was reacted with hydroiodic acid (HI) 57 wt% in water with excess methylamine under nitrogen atmosphere in ethanol with stirring at 0 °C room temperature for 2 h. Typical quantities were 24 mL methylamine, 10 mL HI and 100 mL ethanol. The resultant solution was evaporated to give a white precipitate, then washed with diethyl ether and dried under vacuum and used for the following step without further purication.

### 2.2. Device fabrication

Devices were fabricated on fluorine-doped tin oxide (FTO) coated glass with a sheet resistances of 20 $\Omega\,sq^{-1}$. Initially FTO was removed from regions under the anode contact, to prevent shunting upon contact with measurement pins, by etching the FTO with HCl and zinc powder. Substrates were then cleaned sequentially in soap (2% Hellmanex in water), acetone, ethanol, deionized water and finally treated under oxygen plasma to remove the last traces of organic residues. A compact $TiO_2$ layer was deposited by spin coating a mildly acidic solution of titanium isopropoxide in ethanol (containing 35 μL of 2 M HCl per 5 mL of solution), and annealed at 500 °C for 15 min. The mesoporous $TiO_2$ film was prepared by spin-coating a $TiO_2$ paste (Dyesol 18NR-T) diluted in ethanol with a ratio of 1:3.5 by weight, at 6000 r.p.m. for 30 s, heated at 500 °C for 30 min. The mesoporous $TiO_2$ films were filled by spin-coating of 1 M $PbI_2$ solution in DMF that was kept at 70 °C. After drying at 70 °C, the substrates were spun with 20 μL IPA (2000 r.p.m., 5 s) to undergo pre-wetting. To form the perovskite layer, 0.24 M (35 mg/mL) MAI/IPAs was spin-coated on the $PbI_2$-coated substrate at 4000 r.p.m. for 30 s. Then IPA (200 μl) was spin-coated with repetitions of three times to remove residues. A hole-transporting layer (HTL) was then deposited via spin-coating a 0.79 M solution of spiro-MeOTAD in chlorobenzene, with additives of lithium bis (trifluoromethanesulfonyl) imide and 4-tert-butylpyridine. Devices were then left overnight in air for the spiro-OMeTAD to dope via oxidation (Abate et al., 2013). Finally, 100 nm gold electrodes were deposited on top of the HTL layer through a metal shadow mask via magnetron sputtering with a low current intensity of 5 mA, to finish the fabrication. The active area of cells was defined as 0.1 $cm^2$.

### 2.3. Characterization and measurement

XRD spectra were measured with a Panalytical X'Pert Pro X-ray diffractometer using Cu Kα radiation at 40 kV and 40 mA. A field emission scanning electron microscope (SEM) (Hitachi S-4800) was used to acquire SEM images. The optical properties of perovskite material were studied by Shimadzu UV–visible spectrometry (UV 2600). The current density–voltage ($J$–$V$) curves were measured using a digital source meter (Keithley Model 2400) to apply an external potential bias to the solar cells and measuring the generated photocurrent. The emission spectrum from a 450 W xenon lamp was matched to the standard AM1.5G using a Schott K113 Tempax sunlight filter (Praezisions Glas & Optik GmbH). The exact light intensities of the measurements were determined using a calibrated Si diode as reference.

## 3. Results and discussion

### 3.1. Description of spinning-SSD process

The major steps of spinning-SSD are illustrated in Fig. 1, whose implementation details were described in the section of *Experimental methods*. Compact $TiO_2$ blocking layer and mesoporous $TiO_2$ scaffold were prepared as described in elsewhere (Burschka et al., 2013), followed by spin-coating (not immersing) of MAI/IPAs. This is the primary difference between spinning-SSD and dipping-SSD, by which not only unnecessary materials waste is avoided but also the controllability and facilitation of deposition processing are achieved. In particular, a MAI/IPAs with a concentration as high as 0.24 M was employed for spin-coating, expecting the complete conversion of $PbI_2$. This had been proved to be effective (see below). It is equally important that the pristine IPA was spin-coated both before and after the spin-coating of MAI/IPAs, for which such a process have significant effect on ameliorating the surface morphology and improving the quality of the resulting $MAPbI_3$ films. As above, each step of such procedure was implemented via spin-coating process with a specific quantization parameter, which would contribute to high reproducibility of resulting solar cells. Furthermore, this spinning-SSD process is also expected to achieve mass production of PSCs with a full printable procedure.

### 3.2. Influence of the concentration of MAI/IPAs

Differing from the dipping-SSD process, the spinning-SSD process leads to a film with light surface that can be observed by naked eye because of its good reflectiveness. This advantage is attributed to centrifugal force derived from the high speed spin of substrates, which make the films be with good smoothness. The SEM images and photos of the spinning-SSD process based films, as well as the dipping-SSD process based films are presented in the Supporting Information, Fig. S1. However, it was found that when MAI/IPAs with a lower concentration of 0.063 M (10 mg/mL) was employed, the reaction between $PbI_2$ and MAI was not complete, as unreacted $PbI_2$ was detected. A previous report proved that higher concentration of MAI/IPAs could render the complete conversion of $PbI_2$ into $MAPbI_3$ structure (Chiang et al., 2014). Hence, MAI concentration was increased and 0.24 M was considered as an appropriate value after the parameter optimization. As comparison, MAI/IPAs with concentration of 0.24 M and 0.063 M were used to prepared $MAPbI_3$ structure, and the resulting films were labeled as Film a and Film b, respectively.

Fig. 2 presents the SEM images of these films; their XRD patterns (on glass substrates) and UV–vis spectra (on mesoporous $TiO_2$ layer coated FTO) are shown in Fig. 3. As Fig. 3(a) shows, the diffraction peaks at $2\theta$ values of 14.40, 20.27, 23.78, 24.78, 28.44, 28.73, 31.93, 32.17, 35.26, 40.92, 43.33 and 50.46 degrees were observed both in Film a and Film b, which correspond to the diffraction from (110), (112), (211), (202), (220), (310), (312), (400), (330) and (404) lattice planes of the tetragonal perovskite structure, respectively, similar to the results reported in other reference (Chen et al., 2013; Online et al., 2013; Stoumpos et al., 2013). For Film a, the absence of impurity peaks suggested the complete conversion of $PbI_2$, leading to a final $MAPbI_3$ perovskite films with high crystallization and pure phase. While for Film b, there were two additional peaks at 12.99 and 39.01 degrees, respectively, corresponding to the diffraction from (101) and (110) lattice planes of $PbI_2$ hexagonal polytype, indicating that the conversion of the precursors into $MAPbI_3$ perovskite was incomplete, which would lead to defect of crystal structure and recombination of carriers.

Fig. 3(b) shows the UV–vis spectra of the perovskite films. It can be seen that, both of Film a and b exhibit the similar optical properties with a remarkable absorption

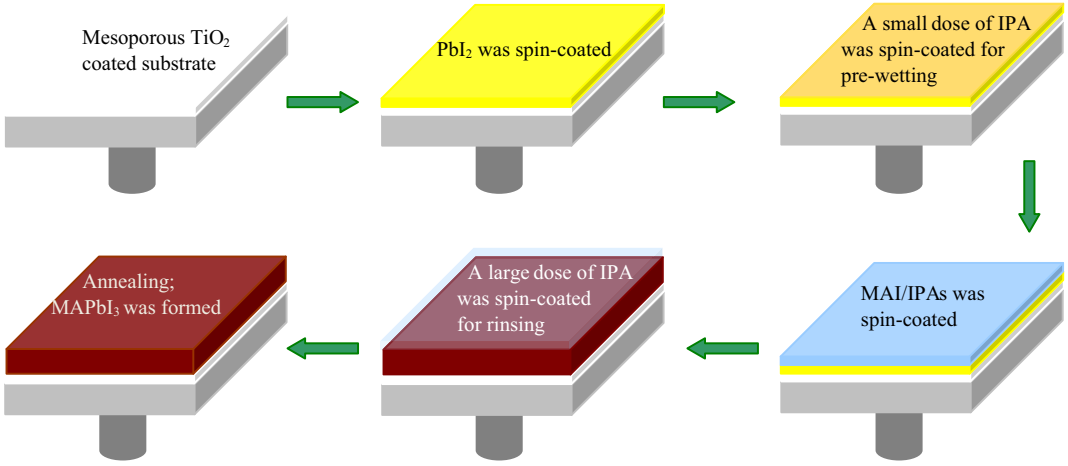


Fig. 1. Spinning-SSD process for fabrication of $MAPbI_3$ films. $PbI_2$ solution is spin-coated onto the mesoporous $TiO_2$ film. A small dose of IPA is spin-coated to undergo a pre-wetting. MAI/IPAs was loaded and spun. A large dose of IPA is spin-coated to remove the residue. Annealing, $MAPbI_3$ was formed.

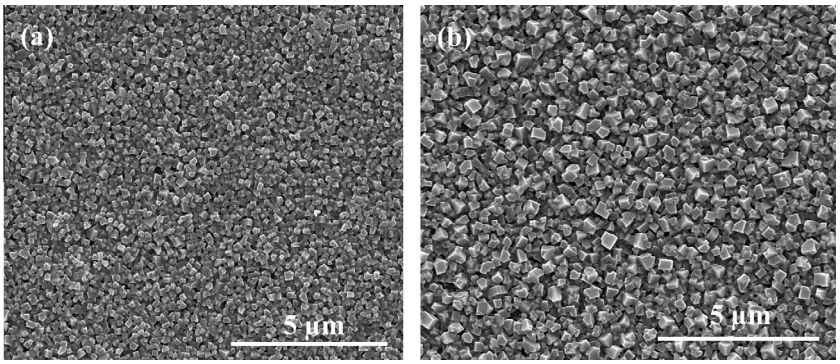


Fig. 2. SEM images of (a) Film a and (b) Film b.

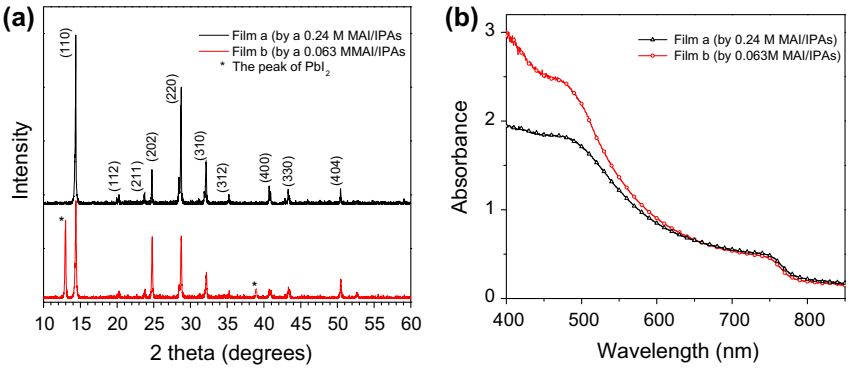


Fig. 3. (a) XRD patterns and (b) UV–vis spectra of Film a and Film b.

decrease near 500 nm and the strong photon harvesting capability over the spectral range from 400 nm to 800 nm, which is in agreement with the band gap of 1.5 eV for $MAPbI_3$ (Haug et al., 2014; Li et al., 2015). As far as the SEM images concerned (Fig. 2), there is a distinct difference between two films. Film a is made up of smaller-sized $MAPbI_3$ grains which grow under the condition of high MAI concentration (Chiang et al., 2014), so it is much more compact. While, Film b is made up of larger-sized $MAPbI_3$ grains which grow under the condition of low MAI concentration (Im et al., 2014; Zheng et al., 2014), leaving some vacant spaces between any two perovskite crystal grains, where mesoporous $TiO_2$ layer is likely to be exposed. It is the right reason that Film b exhibits slightly poorer light-absorption in the range from *ca.* 670 to 800 nm (Fig. 3(b)), although its larger-sized grains lead to better light scattering which would enhance absorption. In additional, a remarkable absorption decreasing in the region from 400 to 450 nm was observed in the UV–vis spectrum of Film b, which is attributed to the characteristic absorbance of the residual $PbI_2$ (Tathavadekar et al., 2015). Therefore, the absence of such an absorption decreasing in the UV–vis spectrum of Film a is reasonable, because the high concentration of MAI/IPAs is helpful for the complete conversion of $PbI_2$. This is consistent with the results of XRD (Fig. 3(a)).

### 3.3. The Role of the spin-coating process of pristine IPA

Both before and after the spin-coating of MAI/IPAs, we spin-coat pristine IPA on the substrates but in a different way, respectively, by which not only the surface morphology of $MAPbI_3$ films were ameliorated but also the quality of it was improved. The former process used a small dose of IPA and employed a low rotating speed (2000 r.p.m., 5 s) to undergo a pre-wetting, by which the larger perovskite grains were formed, enhancing the light harvesting and charge transporting properties of PSCs (Zheng et al., 2014). The SEM images of the resulting $MAPbI_3$ films with or without pre-wetting are presented in Fig. 4(a) and (b), respectively. As it shows, both of them possess high surface coverage, which is of great importance for high performance devices as undesired shunting paths are minimized and thereby maximizing photo-carrier collection (Eperon et al., 2014). It also can be seen that the grains size of perovskite are significantly increased with pre-wetting of IPA, from an average value of 200–500 nm, which is consist with the previous report (Zheng et al., 2014). The latter spin-coating of IPA is implemented after MAI/IPAs was spin-coated, with the purpose to spin-rinse the perovskite films. This step is necessary otherwise there will be residua on the surfaces of perovskite films (as Fig. 4(c) shows), which is residual MAI. To ensure the quality of the films, these

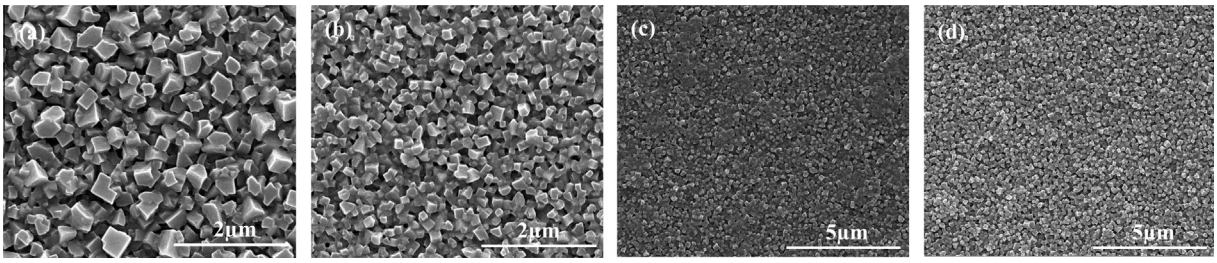


Fig. 4. (a)–(d) Represent the SEM images of $MAPbI_3$ films that pre-wetted with pristine IPA, no pre-wetting, no spin-rinsing and spin-rinsing with pristine IPA, respectively.

residues must be removed. Therefore, a large dose of IPA was needed and dropped dynamically with repetitions of several times for a thorough rinsing, which lead to perovskite films with a flat and uniform surface almost no any residual (see Fig. 4(d)).

### 3.4. Evaluation of photovoltaic performance

The device fabrication was carried out in ambient atmosphere with humidity of less than 30%. More than 60 separate PSCs, with the structure of FTO glass/compact $TiO_2$/mesoporous $TiO_2$/$MAPbI_3$/Spiro-MeOTAD/Au, were fabricated by spinning-SSD process. The statistical histograms of the cell-performance characteristics are presented in Fig. 5. The further statistics indicate the average value of open-circuit voltage ($V_{OC}$), short-circuit current ($J_{sc}$), fill factor (FF) and PCE is 0.94 V, 19.36 mA/cm$^2$, 0.60 and 11.3%, respectively. More importantly, these cells exhibit high reproducibility with a low standard deviation, and the value corresponds to $V_{OC}$, $J_{sc}$, FF and PCE is 0.02, 0.57, 0.58 and 0.52, respectively. The $J$–$V$ characteristics of the cells with the highest-performance and the lowest-performance among these devices are presented in Fig. 6 (a). Such advantages attribute to the reason that the parameters in each step of spinning-SSD procedure are specific and quantitative, by which each process is controlled more precisely, thus leading to the PSCs with good stability of performance.

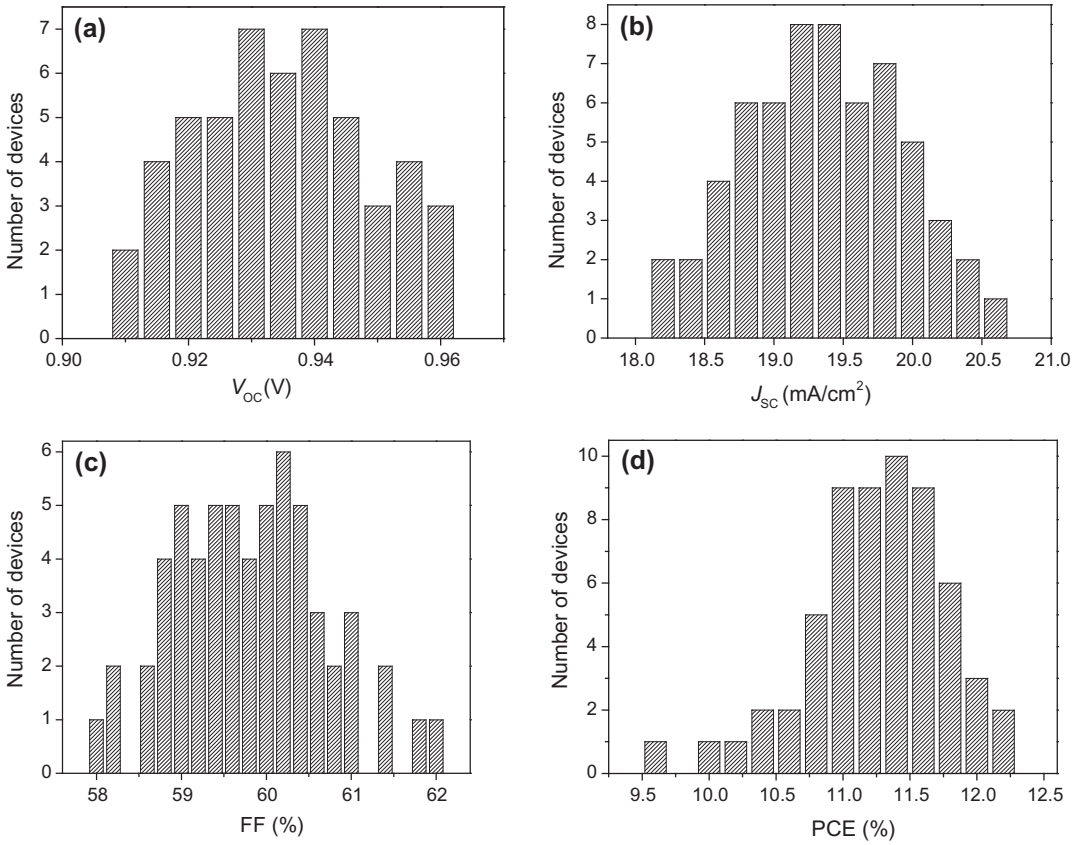


Fig. 5. Histograms of the cell-performance characteristics by measuring 60 separate devices prepared by spinning-SSD process. (a–d) (a) $V_{oc}$, (b) $J_{sc}$, (c) FF and (d) PCE.

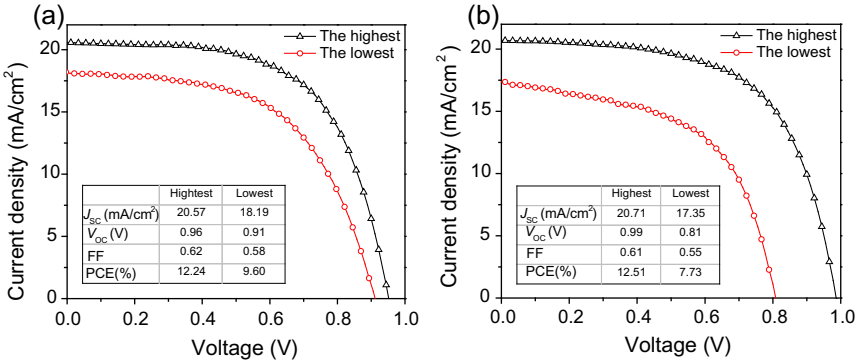


Fig. 6. *J–V* characteristics of the PSCs prepared by (a) spinning-SSD process and (b) dipping-SSD process.

As comparison, the same number of cells with the construct same as the spinning-SSD process based devices were fabricated via the dipping-SSD process. The statistical histograms of the cell-performance characteristics are presented in Supporting Information, Fig. 2S. These 60 dipping-SSD process based devices exhibit an average value of $V_{OC}$, $J_{sc}$, FF and PCE of 0.91 V, 19.17 mA/cm$^2$, 0.58 and 10.4%, respectively, whose *J–V* curves are shown in Fig. 6(b) (the highest-performance one and the lowest-performance one). The standard deviation value of $V_{OC}$, $J_{sc}$, FF and PCE is 0.04, 0.78, 1.44 and 1.17, respectively; each of which is higher than the spinning-SSD process based devices.

The extremum of performance parameters of two batches of PSCs are summarized separately in the inserted table of Fig. 6(a) and (b). It shows clearly that the spinning-SSD process based devices performed better than the devices based on dipping-SSD process. And more excitingly, the spinning-SSD process enhances the reproducibility of PSCs significantly, which indicate the measures we proposed are practical and effective in fabricating high-performance PSCs with high reproducibility.

## 4. Conclusions

In summary, we propose a complete spinning-SSD process to fabricate $MAPbI_3$ perovskite absorption layer, in which several optimization measures are employed, including replacing the dipping and rinsing process with spin-coating process, using MAI/IPAs with high concentration, introducing spin-coating of pristine IPA. This method possesses the advantages of saving materials and operating conveniently, and more importantly, it significantly improves the reproducibility of resulting solar cells because each parameter or condition in such process could be controlled and managed more precisely. By using spinning-SSD process, the resulting meso-structured PSCs exhibited a decent average PCE of 11.3%, with an impressive standard deviation value as low as 0.52. It's worth mentioning that these devices were not fabricated under an optimal condition, so further optimization would contribute to higher performance as well as higher reproducibility. This spinning-SSD process is also expected to achieve mass production of PSCs with a full printable procedure.

## Acknowledgements

This work is supported partially by National High-tech R&D Program of China (863 Program, No. 2015AA034601), National Natural Science Foundation of China (Grant nos. 91333122, 51402106, 51372082, 51172069, 61204064 and 51202067), Ph.D. Programs Foundation of Ministry of Education of China (Grant nos. 20120036120006, and 20130036110012), Par-Eu Scholars Program, and the Fundamental Research Funds for the Central Universities.

## Appendix A. Supplementary material

Supplementary data associated with this article can be found, in the online version, at http://dx.doi.org/10.1016/j.solener.2015.08.028.

## References

Abate, A., Leijtens, T., Pathak, S., Teuscher, J., Avolio, R., Errico, M.E., Kirkpatrik, J., Ball, J.M., Docampo, P., McPherson, I., Snaith, H.J., 2013. Lithium salts as "redox active" p-type dopants for organic semiconductors and their impact in solid-state dye-sensitized solar cells. Phys. Chem. Chem. Phys. 15, 2572–2579. http://dx.doi.org/10.1039/c2cp44397j.

Burschka, J., Pellet, N., Moon, S.-J., Humphry-Baker, R., Gao, P., Nazeeruddin, M.K., Grätzel, M., 2013. Sequential deposition as a route to high-performance perovskite-sensitized solar cells. Nature 499, 316–319. http://dx.doi.org/10.1038/nature12340.

Chen, Q., Zhou, H., Hong, Z., Luo, S., Duan, H.-S., Wang, H.-H., Liu, Y., Li, G., Yang, Y., 2013. Planar heterojunction perovskite solar cells via vapor assisted solution process. J. Am. Chem. Soc. 3–6. http://dx.doi.org/10.1021/ja411509g.

Chiang, C.-H., Tseng, Z.-L., Wu, C.-G., 2014. Planar heterojunction perovskite/PC71BM solar cells with enhanced open-circuit voltage via a (2/1)-step spin-coating process. J. Mater. Chem. A 2, Ahead of Print. http://dx.doi.org/10.1039/C4TA03674C.

Eperon, G.E., Burlakov, V.M., Docampo, P., Goriely, A., Snaith, H.J., 2014. Morphological control for high performance, solution-processed planar heterojunction perovskite solar cells. Adv. Funct. Mater. 24, 151–157. http://dx.doi.org/10.1002/adfm.201302090.

Haug, F., Yum, J., Ballif, C., 2014. Organometallic Halide Perovskites: Sharp Optical Absorption Edge and Its Relation to Photovoltaic Performance.

Im, J., Jang, I., Pellet, N., Park, N., 2014. Size for high-ef fi ciency perovskite solar cells 1–6. http://dx.doi.org/10.1038/nnano.2014.181.

Jeon, N.J., Noh, J.H., Yang, W.S., Kim, Y.C., Ryu, S., Seo, J., Seok, S.II., 2015. Compositional engineering of perovskite materials for high-performance solar cells. Nature. http://dx.doi.org/10.1038/nature14133.

Kim, H.-S., Lee, C.-R., Im, J.-H., Lee, K.-B., Moehl, T., Marchioro, A., Moon, S.-J., Humphry-Baker, R., Yum, J.-H., Moser, J.E., Grätzel, M., Park, N.-G., 2012. Lead iodide perovskite sensitized all-solid-state submicron thin film mesoscopic solar cell with efficiency exceeding 9%. Sci. Rep. 2, 1–7. http://dx.doi.org/10.1038/srep00591.

Kojima, A., Teshima, K., Shirai, Y., Miyasaka, T., 2009. Organo metal halide perovskites as visible-light sensitizer for photovoltaic cells. Priv. Commun. 1, 1. http://dx.doi.org/10.1021/Ja809598.

Lee, M.M., Teuscher, J., Miyasaka, T., Murakami, T.N., Snaith, H.J., 2012. Efficient hybrid solar cells based on Meso-superstructured organometal Halide perovskites. Science (80-.). 338, 643–647. http://dx.doi.org/10.1126/science.1228604.

Li, Y., Cooper, J.K., Giannini, C., Liu, Y., Toma, F.M., Sharp, I.D., 2015. Fabrication of Planar Heterojunction Perovskite Solar Cells by Controlled Low-Pressure Vapor Annealing. http://dx.doi.org/10.1021/jz502720a.

Liu, M., Johnston, M.B., Snaith, H.J., 2013. Efficient planar heterojunction perovskite solar cells by vapour deposition. Nature 501, 395–398. http://dx.doi.org/10.1038/nature12509.

Online, V.A., Baikie, T., Fang, Y., Kadro, J.M., Schreyer, M., Wei, F., Mhaisalkar, S.G., Graetzel, M., White, T.J., 2013. J. Mater. Chem. A, 5628–5641. http://dx.doi.org/10.1039/c3ta10518k.

Stoumpos, C.C., Malliakas, C.D., Kanatzidis, M.G., 2013. Semiconducting tin and lead iodide perovskites with organic cations: phase transitions, high mobilities, and near-infrared photoluminescent properties. Inorg. Chem. 52, 9019–9038. http://dx.doi.org/10.1021/ic401215x.

Tathavadekar, M.C., Agarkar, S.A., Game, O.S., Bansode, U.P., 2015. ScienceDirect Enhancing efficiency of perovskite solar cell via surface microstructuring: superior grain growth and light harvesting effect. Sol. Energy 112, 12–19. http://dx.doi.org/10.1016/j.solener.2014.11.016.

Xiao, Z., Bi, C., Shao, Y., Dong, Q., Wang, Q., Yuan, Y., Wang, C., Gao, Y., Huang, J., 2014. Efficient, high yield perovskite photovoltaic devices grown by interdiffusion of solution-processed precursor stacking layers. Energy Environ. Sci. Ahead of Print. http://dx.doi.org/10.1039/c4ee01138d.

Yang, W.S., Noh, J.H., Jeon, N.J., Kim, Y.C., Ryu, S., Seo, J., Seok, S.II., 2015. High-performance photovoltaic perovskite layers fabricated through intramolecular exchange. Science 348, 1234–1237. http://dx.doi.org/10.1126/science.aaa9272.

Zhao, Y., Nardes, A.M., Zhu, K., 2014. Mesoporous perovskite solar cells: material composition, charge-carrier dynamics, and device characteristics. Faraday Discuss. 176, 301–312. http://dx.doi.org/10.1039/C4FD00128A.

Zheng, L., Ma, Y., Chu, S., Wang, S., Qu, B., Xiao, L., Chen, Z., Gong, Q., Wu, Z., Hou, X., 2014. Improved light absorption and charge transport for perovskite solar cells with rough interfaces by sequential deposition. Nanoscale 6, 8171–8176. http://dx.doi.org/10.1039/c4nr01141d.